ACS Catalysis

Article

Selective hydrogenolysis of #-C-O bond in biomass-derived 2-furancarboxylic acid to 5-hydroxyvaleric acid on supported Pt catalysts at near-ambient temperature

Qianhui Sun, Shuai Wang, and Haichao Liu

ACS Catal., **Just Accepted Manuscript** • DOI: 10.1021/acscatal.9b04074 • Publication Date (Web): 30 Oct 2019

is published by the American Chemical Society. 1155 Sixteenth Street N.W., Washington, DC 20036

Selective hydrogenolysis of α-C-O bond in biomass-derived 2-furancarboxylic acid to 5-hydroxyvaleric acid on supported Pt catalysts at near-ambient temperature

Qianhui Sun[a,b,†], Shuai Wang[c,†], and Haichao Liu[a,]*

[a] Beijing National Laboratory for Molecular Sciences, College of Chemistry and Molecular Engineering, Peking University, Beijing 100871, China

[b] Research Institute of Petroleum Processing, SINOPEC, Beijing 100083, China

[c] State Key Laboratory for Physical Chemistry of Solid Surfaces, Collaborative Innovation Center of Chemistry for Energy Materials, and National Engineering Laboratory for Green Chemical Productions of Alcohols-Ethers-Esters, College of Chemistry and Chemical Engineering, Xiamen University, Xiamen 361005, China

ABSTRACT: Hydrogenolysis of α-C-O bond in abundantly available biomass-based furfural and its derivatives provides a viable route for sustainable synthesis of valuable C5 compounds particularly with two terminal oxygen-containing functional groups. However, efficient cleavage of this bond under mild conditions still remains a crucial challenge, primarily due to the competing cleavage of δ-C-O bond and hydrogenation of furan ring. Here, we report that supported Pt catalysts were extremely active for the selective α-C-O cleavage in 2-furancarboxylic acid (FCA) hydrogenolysis to synthesize 5-hydroxyvaleric acid

(5-HVA), affording a high yield (~78%) on Pt/SiO_2 with a Pt particle size of 4.2 nm at an unprecedentedly low temperature of 313K. In this reaction, the turnover rate and 5-HVA selectivity sensitively depend on the size of the Pt nanoparticles and underlying support, as a consequence of their effects on the exposed Pt surfaces. Combined reaction kinetic, infrared spectroscopic and theoretical assessments reveal that while the exposed high-index Pt surfaces (containing higher fraction of step sites) facilitate the kinetically-relevant addition of the first H atom to the unsaturated C atom in furan ring and thus the hydrogenolysis activity, the low-index surfaces (containing higher fraction of terrace sites), together with the electron-withdrawing effect of the carboxylic substituent in FCA, favorably stabilize the dangling C2 atom in the transition states of α-C-O cleavage and lower their activation barriers, leading to the observed high 5-HVA selectivity. Such pivotal roles of the intrinsic properties of metal surfaces and substituents in tuning the reaction pathways will provide a viable strategy for highly selective upgrading of furan derivatives and other biomass-based oxygenates.

KEYWORDS: selective hydrogenolysis, 2-furancarboxylic acid, 5-hydroxyvaleric acid, Pt catalyst, exposed surface effect, substituent effect

1. INTRODUCTION

Aliphatic compounds with two terminal oxygen-containing functional groups, such as adipic acid and 1,4-butanediol, are important commodity chemicals with versatile applications particularly as monomers in the production of polyesters and polyurethanes, etc.[1,2] While they are commercially manufactured from non-renewable fossil resources,

increasing attention has been paid recently to exploring alternative routes for sustainable synthesis of these important chemicals from biomass-derived feedstocks.[3-5] As such, largely available furfural and its derivatives represent promising precursors because of their structural advantage. For example, via specific cleavage of its α-C-O bond (i.e. the C-O bond in the furan ring at the α position of the CHO group), furfural can be converted to 1,5-pentanediol (1,5-PeD), and by further oxidation even to 1,5-pentanedioic acid.[6]

However, selective activation of the α-C-O bond in the furan ring still remains challenging.[7,8] From the recent studies on hydrogenolysis of furfural[9-11] and its derivatives, furfuryl alcohol (FA)[12-17] and tetrahydrofurfuryl alcohol (THFA)[18-20], it is clear that the formation of 1,5-PeD in these reactions is significantly limited by the competing reaction channels, mainly including parallel hydrogenolysis of δ-C-O bond to 1,2-pentanediol (1,2-PeD) and hydrogenation of the furan-ring on metal catalysts. For example, furfural hydrogenolysis on Pt/CeO_2 formed 57.8% 1,2-PeD and 28.3% THFA with only 4.0% 1,5-PeD at 100% conversion (443 K, 1.0 MPa H_2).[11] In FA hydrogenolysis, a 1,5-PeD selectivity of ~44% was obtained on Cu-based catalysts in ethanol with 1,2-PeD as a major by-product (~18% at 100% conversion).[15] On the other hand, high 1,5-PeD yields (~80%) were recently reported in THFA hydrogenolysis (393 K, 8.0 MPa H_2),[18,21] in which acidic ReO_x-modified Rh or Ir catalysts and high H_2 pressures were however applied to activate THFA due to its high chemical stability. These studies clearly show that more effective catalysts are highly desirable for selectively breaking the α-C-O bond in furfural and its derivatives under mild conditions.

Here, we report hydrogenolysis of 2-furancarboxylic acid (FCA) to synthesize

5-hydroxyvaleric acid (5-HVA) on supported Pt catalysts. FCA can be readily formed from furfural via oxidation or Cannizaro disproportionation.[22-24] 5-HVA is an important compound, and it can be efficiently converted to 1,5-PeD (via hydrogenation), 1,5-pentanedioic acid (via oxidation), and δ-valerolactone (via dehydration), etc., all being useful monomers in synthesis of polymers.[25-27] However, catalytic conversions of FCA into valuable products, especially 5-HVA, have received limited attention and achieved limited success to date.[28,29] In this work, we find that the cleavage of the α-C-O bond can be facilitated by the strong electron-withdrawing effect of -C(=O)OH substituent at the α-C position in FCA, and achieve high 5-HVA yields on supported Pt catalysts at near-ambient temperatures and mild H_2 pressures. Reaction kinetic, spectroscopic, and theoretical methods are combined to further assess the effects of Pt facets on FCA hydrogenolysis activity and selectivity, revealing that the terrace sites predominantly present on low-index Pt surfaces provide extra Pt sites to stabilize the dangling C atom in the transition state of α-C-O cleavage, and account for the high 5-HVA selectivity. This work demonstrates an effective strategy of tuning reaction selectivity via control of exposed metal catalyst surfaces and coordination of functional groups in the oxygenate reactants, generally useful for developing novel routes to catalytic upgrading of biomass feedstocks.

2. EXPERIMENTAL SECTION

2.1. Catalyst Preparation. Pt, Ru, Pd and Ir nanoparticles supported on oxides, including TiO_2 (P25, 99%, Evonik), ZrO_2 (monoclinic, 99%, Alfa Aesar) and SiO_2 (99%, Alfa Aesar), were prepared by a deposition-precipitation method, using $H_2PtCl_6 \cdot 6H_2O$ (A.R.),

$RuCl_3 \cdot 3H_2O$ (A.R.), $PdCl_2$ (A.R.) and $H_2IrCl_6 \cdot 6H_2O$ (A.R.) as the metal precursors, respectively (all purchased from Sinopharm Chemicals). Taking the Pt/TiO_2 catalyst as an example for the catalyst preparation procedure, a certain amount of TiO_2 was added into a diluted aqueous solution of $H_2PtCl_6 \cdot 6H_2O$, into which, under vigorous stirring at a speed of 700 rpm at 333 K, a diluted ammonia solution was added dropwise until the pH value of the solution was over 11. After agitation for 8 h at 333K, the supported catalyst precursors in the solution were centrifugally separated, and then fully washed using deionized H_2O and ethanol. Afterwards, the resulting powders were treated in a vacuum oven at 333 K overnight, heated in flowing air (40 mL min^{-1}) at 623 K (at a ramping rate of 5 K min^{-1}) for 3 h, and subsequently treated in flowing 20% H_2/N_2 (>99.99%, Beijing Huayuan, 40 mL min^{-1}) at 373 K (at a ramping rate of 5 K min^{-1}) for 1 h.

Pt particle sizes of the Pt/SiO_2 catalysts were modulated by changing Pt loadings and thermal treatment conditions of the dried precursors (Table 1), and the catalysts were denoted as Pt/SiO_2-*X*nm, where *X*nm represents the average Pt particle size.

Table 1. Specific preparation protocols for Pt/SiO_2 catalysts with different Pt particle sizes

Catalyst	Pt loading[a] (%)	Thermal treatment[b]	Pt particle size[c] (nm)
Pt/SiO_2-2.6nm	2.0	1. in 20% H_2/N_2 at 523 K for 6 h.	2.6±0.4
Pt/SiO_2-4.2nm	2.0	1. in air at 623 K for 3 h; 2. in 20% H_2/N_2 at 373 K for 1 h.	4.2±0.7
Pt/SiO_2-5.7nm	3.9	1. in air at 673 K for 4 h; 2. in 20% H_2/N_2 at 373 K for 1 h.	5.7±1.3
Pt/SiO_2-7.5nm	5.7	1. in air at 673 K for 4 h; 2. in 20% H_2/N_2 at 373 K for 1 h.	7.5±1.5

[a]Measured by inductively coupled plasma atomic emission spectrometry (ICP-AES). [b]The flow rate of 20% H_2/N_2 and air is 40 mL min^{-1}, and the heating rate of each treatment is 5 K min^{-1}. [c]Measured by transmission

electron microscope (TEM).

2.2. Catalyst Characterization. The compositions of catalysts were measured by inductively coupled plasma atomic emission spectrometry (ICP-AES; Teledyne Leeman Laboratories). X-ray diffraction (XRD) patterns for supported noble metal catalysts were collected on a Rigaku D/MAX-2400 diffractometer within the 2θ range of 10°-80°, using Cu $K_{\alpha 1}$ radiation (λ = 1.5406 Å), operated at 40 kV and 100 mA. The noble metal particle sizes of the catalysts were measured by transmission electron microscope (TEM). TEM images were obtained at an acceleration voltage of 300 kV on Philips Tecnai F30 FEGTEM. Dispersions of Pt particles were calculated by a simplified formula assuming spherical particles and a Pt atom density of 1.25×10^{19} atoms m^{-2},[30] which is given by

$$\text{Pt dispersion} = 1.13/\text{Pt particle size} \quad (1)$$

CO *in-situ* diffuse reflectance infrared Fourier transform spectra (CO-DRIFTS) were collected by averaging 100 scans in the 650-4000 cm^{-1} range with a 2 cm^{-1} resolution on a Bruker Tensor-27 Fourier infrared spectrometer equipped with a Hg-Cd-Te (MCT) detector. Fresh samples (~0.05 g) were treated in an *in-situ* diffuse reflectance cell (Harrick Scientific Products Inc.) in flowing He (20 mL min^{-1}) at 573 K for 0.5 h to eliminate absorbed H_2O and other impurities on the surface by the unavoidable exposure to ambient air, and cooled to 298 K for background spectra collection. The treated samples were exposed in flowing 5% CO/He (20 mL min^{-1}) at room temperature for 0.5 h, and then purged by a He flow (20 mL min^{-1}) for 0.5 h to remove physically absorbed CO before CO-DRIFTS measurements at 298 K.

2.3. Hydrogenolysis reactions of 2-furancarboxylic acid (FCA). Catalytic reactions

were carried out in a 40 mL Teflon-lined stainless steel autoclave with vigorous stirring at a speed of 700 rpm. A certain amount of FCA (A.R., J&K) and fresh catalyst were added into the autoclave and diluted with 10 mL deionized water. The autoclave was pressurized with H_2 (>99.99%, Beijing Huayuan) after fully purging out the air, and heated to the reaction temperatures (313-373 K) monitored by a thermocouple inserted in the autoclave. The concentrations of FCA and hydrogenolysis products were quantified by high-performance liquid chromatography (HPLC; Shimadzu LC-20A) using a RID detector and an Alltech OA-1000 organic acid column (0.001 mol L^{-1} H_2SO_4 mobile phase, 0.6 mL min^{-1} flow rate, and 323 K oven temperature). Turnover rates (mol_{FCA} $(mol_{surface\text{-}Pt} \cdot h)^{-1}$) were reported as molar FCA conversion rates per mole of exposed Pt atoms (estimated from the TEM images as described in Section 2.2), and product selectivities were reported on a carbon basis. For recycling tests, the used catalysts were fully washed with deionized H_2O and acetone, treated in flowing air (40 mL min^{-1}) at 573 K (5 K min^{-1}) for 3 h after drying in a vacuum oven at ambient temperature, and then directly used in the next cycle.

2.4. Computational Methods. Theoretical treatments of the elementary steps involved in FCA hydrogenolysis on Pt(111) and Pt(211) surfaces were carried out using periodic plane-wave density functional theory (DFT) methods[31,32] with the Perdew-Burke-Ernzerhof (PBE) exchange-correlation functional[33] as implemented in the Vienna ab initio simulation package (VASP). The $5d^96s^1$, $2s^22p^4$, $2s^22p^2$, and $1s^1$ electrons were treated explicitly for Pt, O, C and H atoms; core electrons were treated using projector augmented-wave (PAW) pseudo-potentials with an energy cutoff of 400 eV.[34] The Monkhorst-Pack sampling method[35] was used to generate the k-mesh for integration of the first Brillouin zone (i.e. 3×3×1 for

Pt(111) and Pt(211) surfaces). The energy between successive self-consistent iterations was converged to 1×10^{-4} eV, while the structures were optimized until forces were below 0.04 eV Å^{-1}.

Nudged elastic band (NEB)[36] and dimer[37] methods were used to optimize transition state (TS) structure and energy for each elementary step. The starting point for each TS structure was obtained by NEB method with 8 images along the reaction coordinate. The electronic structures were converged self-consistently to energies of 1×10^{-3} eV using a single Γ-centered k-point, and the corresponding maximum force on each atom converged to 0.1 eV Å^{-1}. The starting TS structure was then optimized by the dimer method, using a 3×3×1 Monkhorst-Pack k-point mesh and more stringent convergence criteria for electronic energies and forces (1×10^{-4} eV and 0.04 eV Å^{-1}, respectively).

The experimental lattice constants (3.92 Å) of crystalline Pt[38] were used to build Pt(111) and Pt(211) surfaces. The Pt(111) and Pt(211) surfaces were modeled by 4 atomic-layer slabs, which were repeated in 3×3 and 1×4 surface supercells, respectively. During all calculations, the bottom two layers of Pt(111) and three layers of Pt(211) were fixed to the bulk positions, while the rest layers were allowed to fully relax. To avoid interactions between slabs, all slabs were separated by a vacuum gap of 20 Å.

The adsorption energy (E_{ads}) of an adsorbate to the surface slabs was calculated as follows:

$$E_{ads} = E_{slab+i} - E_{slab} - E_i \qquad (2)$$

where E_{slab+i}, E_{slab}, and E_i are the DFT-derived electronic energies of the adsorption complex, clean surface slab and gas-phase adsorbate *i*, respectively. The reaction activation barriers

(E_a) were calculated as follows:

$$E_a = E_{TS} - E_{IS} \quad (3)$$

where E_{TS} and E_{IS} were the DFT-derived electronic energies of the transition state and the initial state of a given elementary reaction, respectively.

3. RESULTS AND DISCUSSION

3.1. Activity and Selectivity of Aqueous-Phase 2-Furancarboxylic Acid Hydrogenolysis on Supported Metal Catalysts. TiO_2-supported Pt, Ru, Pd and Ir catalysts with similar metal particle sizes of ~2 nm (TEM micrographs shown in Fig. 1a-d) were prepared by a deposition precipitation method, and used to examine the intrinsic selectivity of FCA hydrogenolysis on different noble metal catalysts. As shown in Table 2, on Pt/TiO_2, FCA hydrogenolysis formed 5-HVA and THFCA with selectivities of 59.3% and 38.0% at ~26% conversion, respectively, at 313 K and 3 MPa H_2. Their selectivities kept almost constant within the whole range of FCA conversions (15-100%, Fig. S1a, SI), indicating that both 5-HVA and THFCA are the primary products. We thus surmise that 5-HVA was formed from direct hydrogenolysis of the α-C-O bond in FCA, instead of secondary C-O hydrogenolysis of THFCA after the furan ring in FCA was completely saturated (Scheme 1). The THFCA hydrogenolysis pathway for 5-HVA formation appears to be kinetically unfavorable because of the low ring-opening reactivity of THFCA, most likely due to the weak adsorption of THFCA on the Pt surface through its tetrahydrofuran ring. It is worth noting that no ring-opening products derived from hydrogenolysis of the δ-C-O bond in FCA (e.g. 2-hydoxyvaleric acid) were detected, reflecting the preferential cleavage of the α-C-O

bond in FCA conferred by the strong electron-withdrawing effect of the carboxylic group attached to the α-C atom. Such hydrogenolysis selectivities for the furan-ring C-O bonds on Pt catalysts were completely different when the carboxylic substituent was replaced by an electron-denoting hydroxy methyl group (i.e. furfural alcohol as reactant),[13] as discussed in the introduction section, and also observed in our control experiments that showed similar selectivities for the cleavage of α-C-O and δ-C-O bonds on the Pt catalysts (313 K, 3 MPa H_2; Fig. S2, SI).

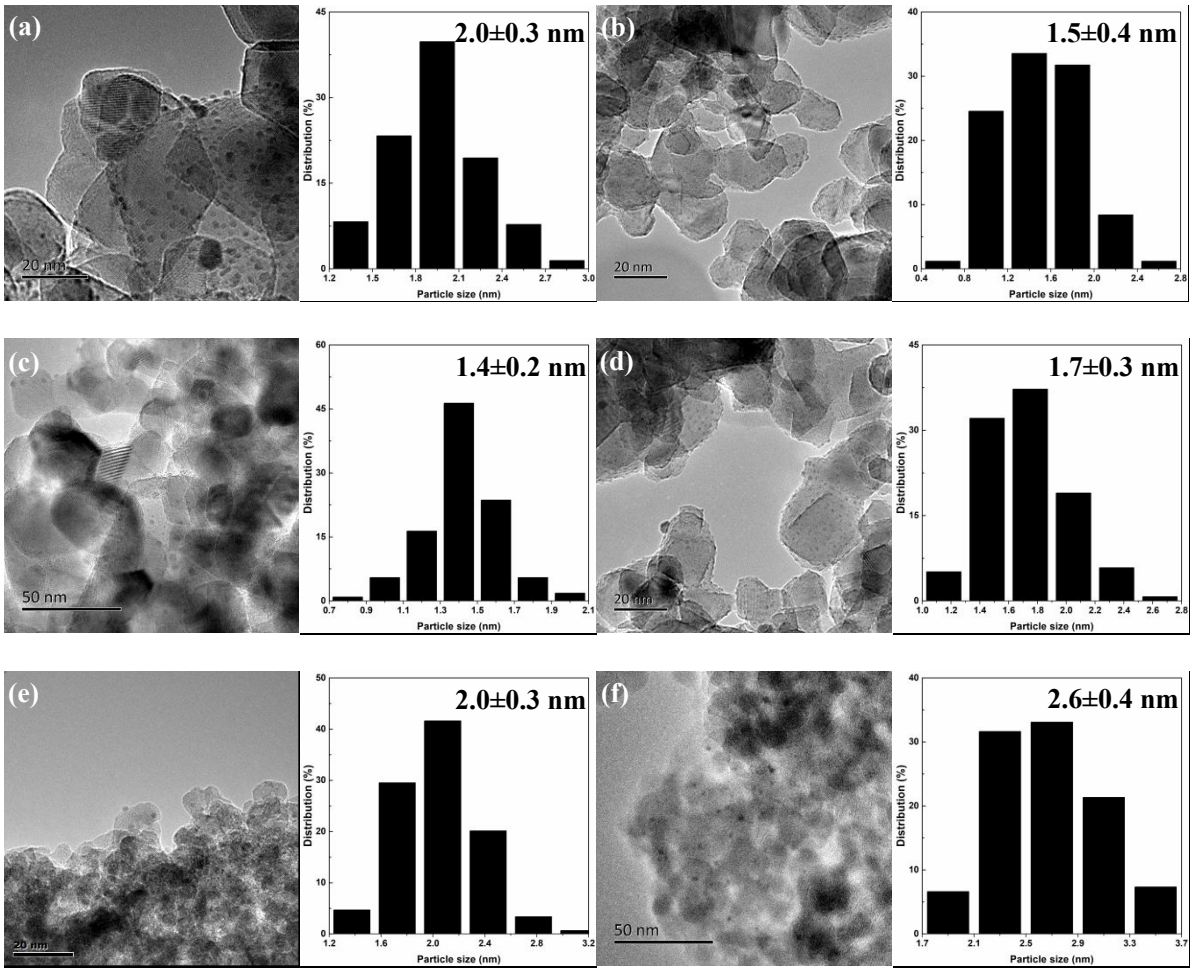

Figure 1. Transmission electron microscopy (TEM) micrographs and histograms of metal particle size distribution for (a) 2% Pt/TiO_2, (b) 2% Ru/TiO_2, (c) 2% Pd/TiO_2, (d) 2% Ir/TiO_2, (e) 2% Pt/ZrO_2, (f) 2% Pt/SiO_2-2.6nm (prepared by the protocol described in Section 2.1)

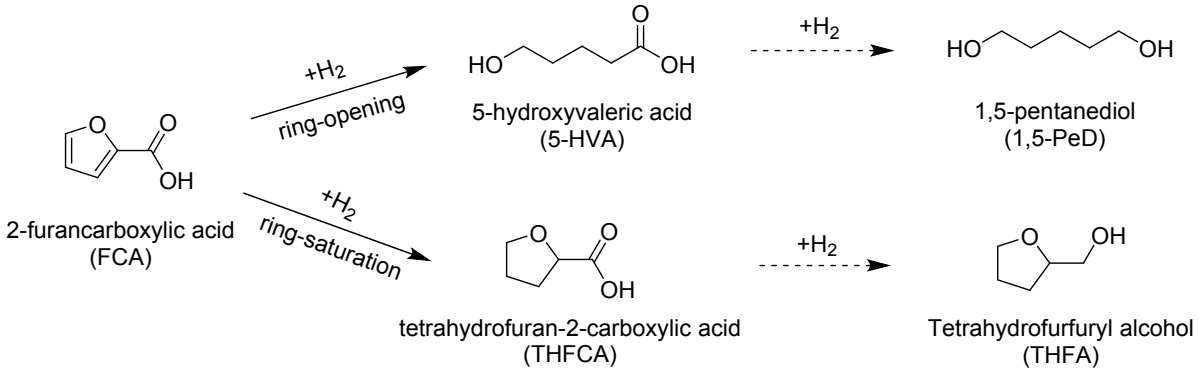

Scheme 1. Ring-opening and ring-saturation pathways for FCA hydrogenolysis on Pt catalysts.

Table 2. Selectivities of FCA hydrogenolysis on Pt, Ru, Pd, and Ir-based catalysts.

Catalyst	Particle size (nm)	Conversion (%)	Selectivity (on a carbon basis, %)			
			5-HVA[c]	1,5-PeD[d]	THFCA[e]	THFA[f]
2%Pt/TiO_2	2.0±0.3	25.7[a]	59.3	n.d.	38.0	n.d.
		96.6[b]	57.3	3.6	39.2	n.d.
2%Ru/TiO_2	1.5±0.4	91.9[b]	10.4	0.4	87.9	1.3
2%Pd/TiO_2	1.4±0.2	100[b]	n.d.	n.d.	99.9	n.d.
2%Ir/TiO_2	1.7±0.3	95.3[b]	n.d.	n.d.	97.5	n.d.

Reaction conditions: [a] 0.5 g FCA in 10 mL water, 0.1 g catalyst, 313 K, 3 MPa H_2, 3 h; [b] 0.5 g FCA in 10 mL water, 0.2 g catalyst, 373 K, 4 MPa H_2, 10 h; [c] 5-HVA = 5-hydroxyvaleric acid; [d] 1,5-PeD = 1,5-pentanediol; [e] THFCA = tetrahydrofuran-2-carboxylic acid; [f] THFA = tetrahydrofurfuryl alcohol.

Even at 373 K and nearly complete FCA conversion (96.6%), the selectivities to 5-HVA and THFCA on Pt/TiO_2 remained essentially unchanged (at 57.3% and 39.2%, respectively; Table 2), although a small amount of 1,5-PeD (3.6% selectivity) was formed via secondary hydrogenation of 5-HVA (Scheme 1). In contrast, the main product of FCA hydrogenolysis on Ru/TiO_2 was THFCA (87.9% selectivity), and the 5-HVA selectivity decreased to 10.4% (Table 2). On Pd/TiO_2 and Ir/TiO_2, THFCA was almost exclusively formed from FCA

reaction (selectivity > 97%). The different selectivity on these catalysts with similar metal particle sizes reflects that the relative abilities for catalyzing C-O bond cleavage and C=C bond hydrogenation are sensitive to the nature of metal sites. Such selectivity dependence appears to be relevant to the oxygen affinity of the metal sites that determines the accessibility of the furan-ring O atom in the hydrogenolysis process as suggested from the following theoretical calculations shown in Section 3.4. Only on Pt surface, which has a lower oxygen affinity than the other VIII group metals,[39] the C-O bond cleavage is preferred over the C=C bond hydrogenation, exhibiting the uniquely high selectivity to 5-HVA in FCA hydrogenolysis (Table 2).

Figure 2 compares reaction rates and selectivities of FCA hydrogenolysis on TiO_2, ZrO_2 and SiO_2-supported Pt particles of ~2 nm (TEM micrographs shown in Fig. 1a, e and f) within the kinetically controlled regime (at ~20% conversion). The three oxide supports are resistant to acid corrosion, making them suitable for FCA hydrogenolysis. Similar to Pt/TiO_2, FCA hydrogenolysis on Pt/ZrO_2 and Pt/SiO_2 showed combined selectivities of 5-HVA and THFCA above 96% at 313 K and 3 MPa H_2, indicating that the hydrogenolysis pathways of FCA on Pt surfaces are not significantly affected by the oxide supports. The FCA reaction rates normalized by the exposed surface Pt atoms (i.e. turnover rates) decreased in an order of Pt/TiO_2 (322.0 mol_{FCA} $(mol_{surface\text{-}Pt}\cdot h)^{-1}$), Pt/$ZrO_2$ (168.2 mol_{FCA} $(mol_{surface\text{-}Pt}\cdot h)^{-1}$) and Pt/$SiO_2$ (108.0 mol_{FCA} $(mol_{surface\text{-}Pt}\cdot h)^{-1}$), whereas the corresponding selectivities to 5-HVA on these catalysts were 59.3%, 65.7% and 73.3% (Fig. 2), which indicates that selective formation of 5-HVA requires moderate hydrogenolysis activity. These support effects on catalytic activity and selectivity are ascribable to the change of exposed Pt surfaces determined by the

interaction between Pt particles and oxide support, as evidenced from spectroscopic characterization and theoretical calculations shown below in Sections 3.2 and 3.4, respectively.

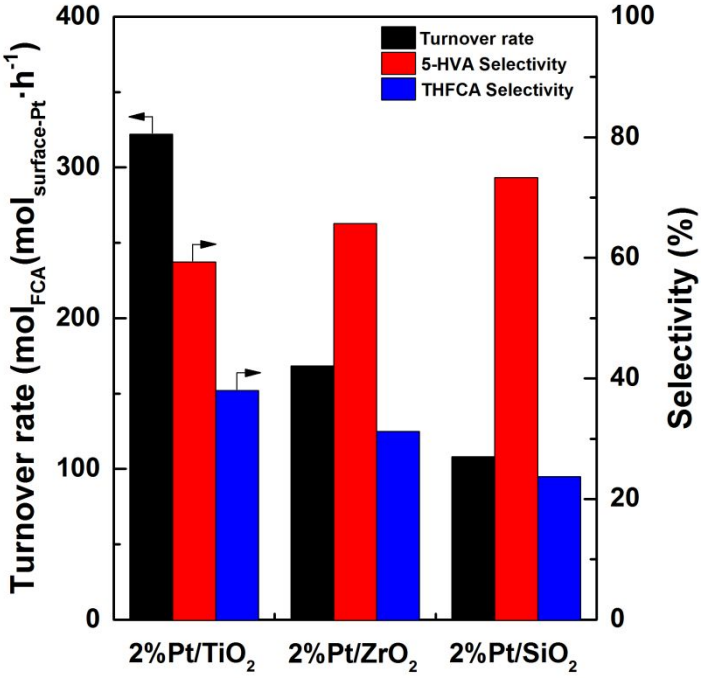

Figure 2. Turnover rates and selectivities of FCA hydrogenolysis on Pt particles supported by TiO_2, ZrO_2, and SiO_2 (0.5 g FCA in 10 mL water, 313 K, 3 MPa H_2, 3 h, ~20 % FCA conversion obtained by varying catalyst amount).

The reaction rates and selectivities of FCA hydrogenolysis are also tunable by changing the size of Pt particles. As depicted in Figure 3, the turnover rates of FCA conversion on Pt/SiO_2 decreased gradually from 108.0 to 99.6 mol_{FCA} $(mol_{surface\text{-}Pt}\cdot h)^{-1}$ at 313 K and 3 MPa H_2 when the average size of Pt particles increased from 2.6 to 7.5 nm (controlled by varying the Pt loading and treatment condition as described in Section 2.1; TEM micrographs shown in Fig. S3, SI). In concomitance with this activity change, the selectivity to 5-HVA increased from 73.3% to 80.0% with increasing the Pt particle size in the examined range, whereas the selectivity to THFCA declined from 23.7% to 17.5%. Such size effects are consistent with

the higher 5-HVA selectivities observed on less active Pt sites (Fig. 2), and thus imply that 5-HVA is favorably formed on lower-index Pt surfaces that generally prevail for larger Pt particles.

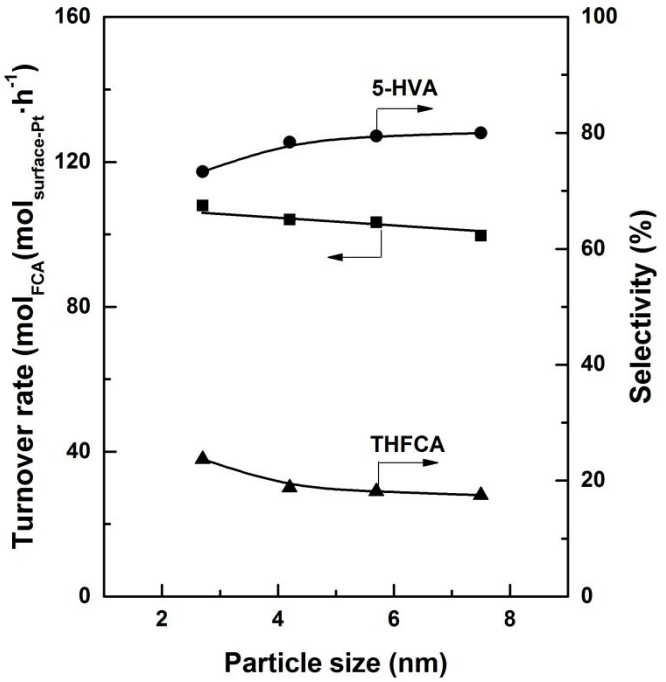

Figure 3. Effects of Pt particle size on turnover rates and selectivities in FCA hydrogenolysis on Pt/SiO_2 (0.5 g FCA in 10 mL water, 313 K, 3 MPa H_2, 3 h, ~20 % FCA conversion obtained by varying catalyst amount).

The above results show that SiO_2-supported Pt particles of moderate sizes (e.g. ~4 nm) are more appropriate for catalyzing FCA hydrogenolysis to produce 5-HVA than other Pt particle sizes or oxide supports, because of the balance between the catalytic activity of FCA hydrogenolysis and the selectivity to 5-HVA. The Pt/SiO_2 catalyst with an average Pt particle size of 4.2 nm remained a high 5-HVA selectivity of 78.1% at ~100% FCA conversion (313 K, 3 MPa H_2; Fig. S1b), reflecting its intrinsically high selectivity to 5-HVA. Moreover, both turnover rate and 5-HVA selectivity of this Pt/SiO_2 sample kept almost unchanged after four consecutive cycles of FCA hydrogenolysis within the kinetically controlled regime (Fig. 4).

No leaching of Pt was detectable in the reaction solution after recycling (by ICP-AES), and the average size of the Pt particles in the spent Pt/SiO_2 catalyst increased slightly to 5.4 nm (TEM micrographs shown in Fig. S4, SI; XRD patterns shown in Fig. S5, SI), consistent with the high stability of Pt/SiO_2 during FCA hydrogenolysis.

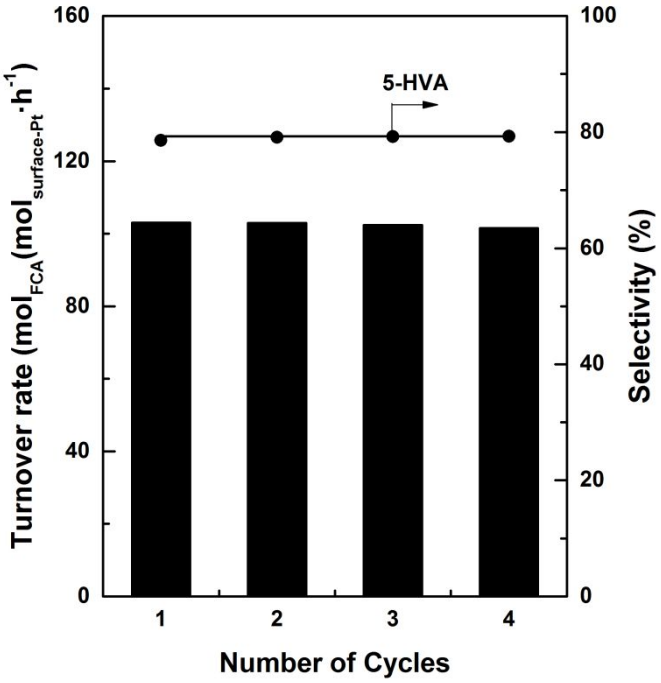

Figure 4. Turnover rates and selectivities to 5-HVA for four consecutive cycles of FCA hydrogenolysis on Pt/SiO_2-4.2nm (0.5 g FCA in 10 mL water, 0.2 g Pt/SiO_2-4.2nm, 313 K, 3 MPa H_2, 3 h).

3.2. Infrared Spectroscopic Assessment of Exposed Pt Sites via CO Adsorption. CO adsorption was used here to discern the Pt sites exposed on the oxide supports, because the vibrational frequency of CO is sensitive to the chemical state of bound metal sites.[40] The stretching bands of adsorbed CO appeared in the range of 2000-2150 cm^{-1} for the Pt/TiO_2, Pt/ZrO_2 and Pt/SiO_2 samples at ambient temperature (Fig. 5a), which are assigned to linearly atop adsorption modes at Pt surface sites.[40] On Pt/TiO_2, adsorbed CO molecules showed vibrational bands at 2037, 2063, 2086 and 2115 cm^{-1}, indicative of different extents of

back-donation of electrons from the Pt surface sites to the CO 2π* orbitals. The lower the CO band frequency is, the higher d-band electron density the exposed Pt sites have. Specifically, the three bands between 2037-2086 cm^{-1} are ascribed to CO adsorption on the metallic Pt sites with different coordination numbers (e.g. those in the terraces, steps, and edges of the exposed Pt surfaces),[41] while the band at 2115 cm^{-1} is ascribed to the CO adsorption on the cationic $Pt^{\delta+}$ sites that are strongly bound to the lattice oxygen of Pt-TiO_2 interfaces.[42,43] Similar CO stretching bands were also observed for Pt/ZrO_2 with slight blue shifts to 2041, 2065, 2090 and 2124 cm^{-1}, respectively.

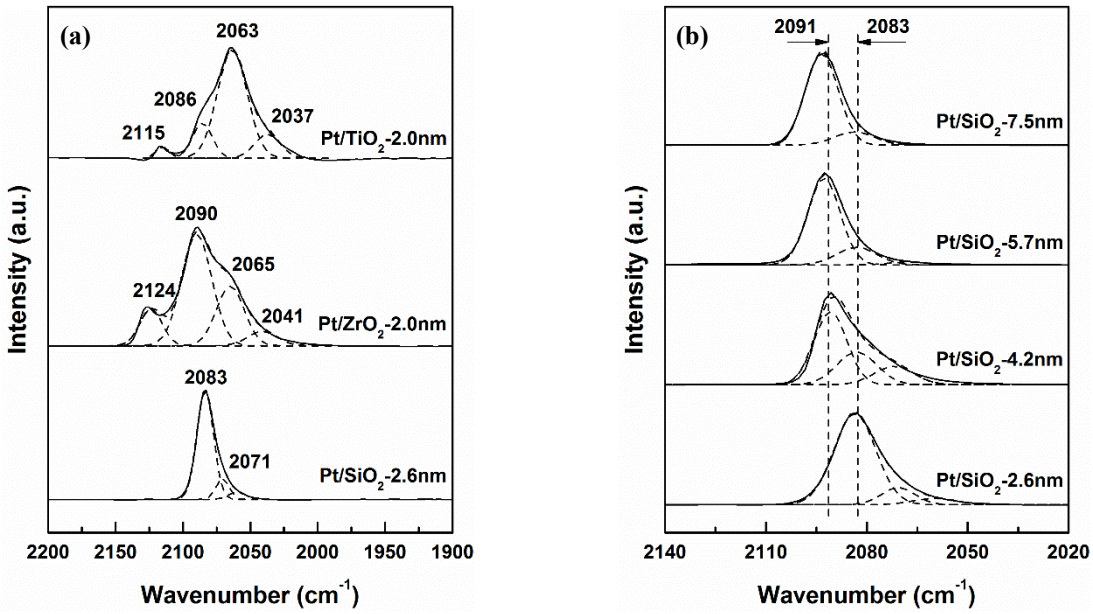

Figure 5. CO-DRIFTS spectra of (a) Pt catalysts on different supports and (b) Pt/SiO_2 with different Pt particle sizes.

In contrast, the CO adsorption on Pt/SiO_2 showed the main vibrational band at 2083 cm^{-1} with a little shoulder at 2071 cm^{-1} (Fig. 5a). The absence of CO bands above 2100 cm^{-1} reflects weak interaction between Pt and SiO_2 in the Pt/SiO_2 sample,[44,45] whereas the low integrated intensity of CO bands below 2070 cm^{-1} suggests that Pt/SiO_2 lacks high-index Pt

surfaces that possess abundant step and corner sites of high d-band electron densities.[41, 46-48] Consistently, the main CO vibrational bands shifted from 2083 to 2091 cm^{-1} as the average Pt particle size of Pt/SiO_2 increased from 2.6 to 7.5 nm (Fig. 5b), and such increase of the Pt particle size leads to higher portion of terrace sites that are predominant on low-index surfaces.[46,47,50]

These observed differences in the infrared spectra of CO adsorption for these supported Pt catalysts imply that the low-index Pt surfaces contribute to the high selectivity of 5-HVA. Next, kinetic and theoretical methods are combined to provide molecular-level insights into this structural requirement of Pt catalysts for selective FCA hydrogenolysis.

3.3. Kinetic Assessment of FCA Hydrogenolysis on Pt catalysts. The effects of reactant concentrations on FCA hydrogenolysis rate and selectivity were examined at 313 K on the Pt/SiO_2 (with Pt particle size of 4.2 nm, donated as Pt/SiO_2-4.2nm) and Pt/TiO_2 (with Pt particle size of 2.0 nm, donated as Pt/TiO_2-2.0nm) catalysts, representing the aforementioned low-index and high-index Pt surfaces, respectively, in order to assess their intrinsic difference in catalyzing FCA hydrogenolysis. As shown in Figure 6a, at similar FCA conversions (~20%), the turnover rates on Pt/SiO_2-4.2nm increased with increasing the concentration of FCA, and then reached a plateau around 100 mol_{FCA} $(mol_{surface\text{-}Pt}\cdot h)^{-1}$ at higher FCA concentrations of above 0.20 mol L^{-1}, reflecting high coverages of FCA or its derived species on the Pt surfaces during catalysis. In contrast, the turnover rates on Pt/TiO_2-2.0nm increased to a maximum value of 335.7 mol_{FCA} $(mol_{surface\text{-}Pt}\cdot h)^{-1}$ with increasing the FCA concentration to 0.08 mol L^{-1}, which then declined gradually as the FCA concentration further increased. We surmise that the adsorption of FCA on the Pt/TiO_2-2.0nm

catalyst is so strong that high FCA concentration can hinder the adsorption and dissociation of H_2 on the same Pt surfaces required for the proceeding of FCA hydrogenolysis, which accounts for the observed decrease of FCA hydrogenolysis rates at FCA concentrations above 0.08 mol L^{-1}. The selectivities to 5-HVA and THFCA were essentially insensitive to the FCA concentration in the examined range (0.039-0.634 mol L^{-1}) for both Pt/SiO_2 and Pt/TiO_2 catalysts (Figs. S6a and S7a, SI), indicating that 5-HVA and THFCA are formed apparently from identical FCA-derived intermediates adsorbed on Pt surfaces with an identical reaction order.

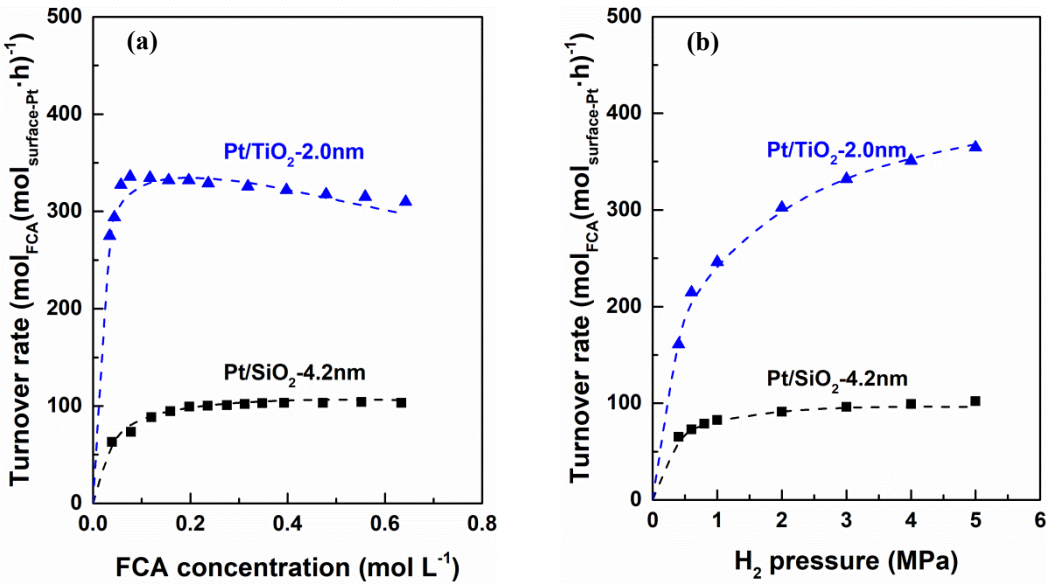

Figure 6. Effects of (a) FCA concentration and (b) H_2 pressure on turnover rates in FCA hydrogenolysis on Pt/SiO_2-4.2nm and Pt/TiO_2-2.0nm (313 K, 3 h, ~20 % FCA conversion obtained by varying catalyst amount; (a) 3.0 MPa H_2; (b) 0.2 g FCA in 10 mL water, i.e., 0.198 mol L^{-1}). Dashed curves represent regressed fits to the functional form of Equation 4.

For the kinetic effects of H_2 pressure on the Pt/SiO_2 and Pt/TiO_2 catalysts (Fig. 6b), increasing H_2 pressure led to an increase of the turnover rates, which then became less sensitive to the H_2 pressures higher than ~1 MPa. This trend indicates that H atoms are readily accumulated on the Pt surfaces under the reaction conditions. Similar to the effect of

FCA concentrations, the selectivities to 5-HVA and THFCA kept nearly constant within a large range of H_2 pressures (1-5 MPa, Figs. S6b and S7b, SI), further supporting that the two products are formed from the identical FCA-derived surface intermediates.

By referring to the previous reports on hydrogenolysis reactions of furan derivatives,[14,51] we propose that FCA hydrogenolysis on Pt surfaces proceeds involving the following elementary steps (Scheme 2). First, FCA adsorbs molecularly on multiple Pt sites that is closely related to the nature of the exposed Pt surface, while a H_2 molecule dissociates on two Pt sites to form H atoms. The H atoms then attack the C=C bonds of the adsorbed FCA, yielding partially hydrogenated intermediates ($FH_n(\alpha^*)$; *n* is the number of added H atoms and α is the number of Pt surface atoms to which each intermediate binds). These $FH_n(\alpha^*)$ intermediates can be further hydrogenated to form THFCA via full saturation of the furan ring or be hydrogenolyzed to form 5-HVA via selectively breaking the C-O bond of the furan ring.

Scheme 2. Proposed sequence of reaction steps for FCA hydrogenolysis on metal surface.[a]

FCA adsorption	$FCA + m^* \rightleftharpoons FCA(m^*)$
H_2 dissociation	$H_2 + 2^* \rightleftharpoons 2H(^*)$
Partial hydrogenation	$FCA(m^*) + nH(^*) \rightarrow FH_n(\alpha^*) + (m+n-\alpha)^*$
Ring-saturation	$FH_n(\alpha^*) + H(^*) \rightarrow FH_{n+1}(\beta^*) + (\alpha+1-\beta)^*$ $FH_{n+1}(\beta^*) + (3-n)H(^*) \rightarrow THFCA + (\beta+4-n)^*$
Ring-opening	$FH_n(\alpha^*) + H(^*) \rightarrow FH_{n+1}\text{-ro}(\beta'^*) + (\alpha+1-\beta')^*$ $FH_{n+1}\text{-ro}(\beta'^*) + (5-n)H^* \rightarrow 5\text{-HVA} + (\beta'+5-n)^*$

[a] *m* represents the average bound Pt atoms per FCA for its adsorption on a given Pt catalyst. FH_n represents the partially hydrogenated intermediates, where *n* is the number of added H

atoms. α or β is the number of Pt surface atoms that each intermediate binds to; FH_n-ro represents the ring-opening intermediate via breaking the C-O bond of the furan ring.

On the assumptions that the addition of the first H atom to the furan ring is the kinetically relevant step[14,51] and the bound FCA and H atom are the prevailing surface species, from the proposed elementary steps, we derived an expression of the FCA hydrogenolysis rate equation as

$$\text{Rate} = \frac{k_{app}[\text{FCA}][\text{H}_2]^{\frac{1}{2}}}{(1 + K_{\text{FCA}}{}^{\frac{1}{\text{m}}}[\text{FCA}]^{\frac{1}{\text{m}}} + K_{\text{H2}}{}^{\frac{1}{2}}[\text{H}_2]^{\frac{1}{2}})^{1+\text{m}}} \qquad (4)$$

Here, k_{app} is the apparent kinetic constant for the H-addition of FCA catalyzed by Pt, K_{FCA} and K_{H2} are the respective equilibrium constants for FCA adsorption and H_2 dissociation on the Pt surfaces, and *m* represents the average bound Pt atoms per FCA for its adsorption on a given Pt catalyst. The measured FCA hydrogenolysis rates obtained on the Pt/SiO_2 and Pt/TiO_2 catalysts fitted well with Equation 4 (Fig.6 and Fig. S8, SI), supporting the kinetic relevance of the addition of the first H atom to the bound FCA species. Furthermore, these data suggest that alternate assumption of the subsequent addition of H atoms to the adsorbed FCA species did not involve in the kinetically relevant steps of FCA hydrogenolysis, because of poor regression fittings for such cases.

The regressed parameters of Equation 4 for the Pt/SiO_2 and Pt/TiO_2 catalysts were compared in Table 3. The k_{app} value of Pt/TiO_2 was about two times higher than that for Pt/SiO_2 (1.5×10^6 *vs*. 5.3×10^5 L mol^{-1} MPa$^{-0.5}$ h^{-1}), reflecting that the Pt sites on the high-index surfaces are intrinsically more active than those on the low-index surfaces. Compared with Pt/SiO_2, such high-index Pt surfaces on Pt/TiO_2 also led to a slight decrease of the average

bound Pt atoms per FCA (m: 2.6 vs. 2.9) and to stronger adsorption of FCA (K_{FCA}: 4.4 ×10^2 vs. 3.6 ×10^2 L mol^{-1}), consistent with the presence of more step sites on the high-index surfaces.[52] On the other hand, the H_2 dissociation constant (K_{H2}) for Pt/TiO_2 was smaller than that for Pt/SiO_2 (K_{H2}: 0.41 vs. 0.78 MPa^{-1}), which implies that the co-adsorption of strongly bound FCA species weakens the stability of H atoms on the high-index Pt surfaces. In spite of such differences in these adsorption constants between Pt/SiO_2 and Pt/TiO_2, their total coverages of bound FCA and H species were always above 80% under the examined reaction conditions, unveiling that FCA hydrogenolysis occurred on densely covered Pt surfaces.

Table 3. Regressed kinetic parameters for FCA hydrogenolysis on Pt/SiO_2-4.2nm and Pt/TiO_2-2.0nm catalysts at 313 K.

Catalyst	k_{app} (L mol^{-1} $MPa^{-0.5}$ h^{-1})	K_{FCA} (L mol^{-1})	K_{H2} (MPa^{-1})	m
Pt/SiO_2-4.2nm	5.3×10^5	3.6×10^2	0.78	2.9
Pt/TiO_2-2.0nm	1.5×10^6	4.4×10^2	0.41	2.6

Based on the above kinetic analysis, the addition of the first H atom to the furan ring determines how fast FCA converts on the Pt surfaces, whereas the kinetic constants of partially hydrogenated FCA intermediates for the branching furan-ring saturation and opening steps determine the selectivities to form THFCA and 5-HVA products. It is worth nothing that the ratios of these kinetic constants can be regarded as a descriptor for the intrinsic selectivities of furan-ring saturation and opening on a given Pt catalyst, which are

directly measurable from experiments and insensitive to the concentrations of FCA and H_2. Specifically, the ratios for Pt/SiO_2 and Pt/TiO_2 are 4.3 and 1.5, respectively (Figs. S6a and S7a, SI), reflecting the higher 5-HVA selectivity on low-index Pt surfaces. However, these ratios are unable to provide molecular details on the relevant surface intermediates, because these H-addition events occur after the kinetic limiting step. Next, theoretical treatments were applied to assess the elementary steps of FCA hydrogenolysis on Pt surfaces and the effects of Pt facets on the hydrogenolysis activity and selectivity.

3.4. Theoretical Assessment of FCA Hydrogenolysis on Pt Surfaces. Theoretical simulations of FCA hydrogenolysis on Pt surfaces were carried out using Pt(111) and Pt(211) planes in order to examine the effects of Pt facets on hydrogenolysis rates and selectivities. Uniform Pt sites with a coordination number (CN) of 9 are exposed on the flat low-index Pt(111) planes, whereas the high-index Pt(211) planes are corrugated surfaces consisting of step (CN: 7), terrace (CN: 9), and corner (CN: 10) sites.[53] Structural optimization of FCA adsorption on the two Pt planes showed that parallel adsorption models via coordination of furan ring to the Pt surface are most stable for both planes. Specifically, FCA prefers to bind to three terrace sites of the Pt(111) surface, but to two step sites of the Pt(211) surface (Fig. 7). Calculated adsorption energies for FCA on Pt(111) and Pt(211) planes were -0.52 and -1.37 eV (Fig. 8), respectively, reflecting stronger stability of adsorbed FCA on the coordinately more unsaturated Pt sites. The corresponding adsorption energies for a H atom on the vicinal Pt sites of the adsorbed FCA molecules were -0.22 eV for Pt(111) and -0.21 eV for Pt(211) (Fig. 8; gaseous H_2 as the energy reference), both of which are much lower than

for FCA. The weaker stability of the adsorbed H atom on Pt(211) than on Pt(111) may be attributed to steric hindrance of the neighboring FCA species that binds more strongly on Pt(211). These stability differences for adsorbed FCA and H-atom on the Pt(111) and Pt(211) planes agree well with those observed from the kinetic assessments on Pt/SiO_2 and Pt/TiO_2 (Section 3.3), indicating that the Pt(111) and Pt(211) planes are suitable models for studying the effects of Pt facets on FCA hydrogenolysis.

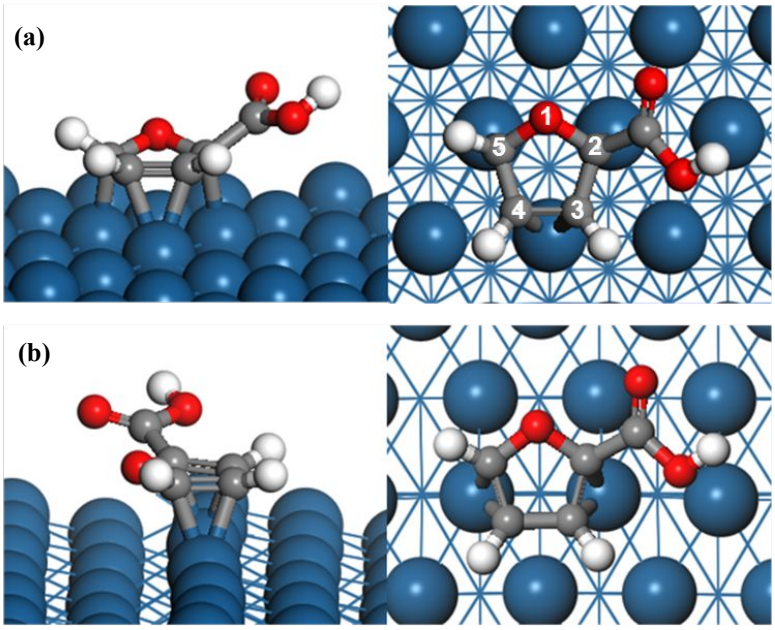

Figure 7. Calculated structures of absorbed FCA on (a) Pt(111) surface and (b) Pt(211) surface. (Atom legend: Pt, blue; C, gray; O, red; H, white; some specific atoms are labeled.)

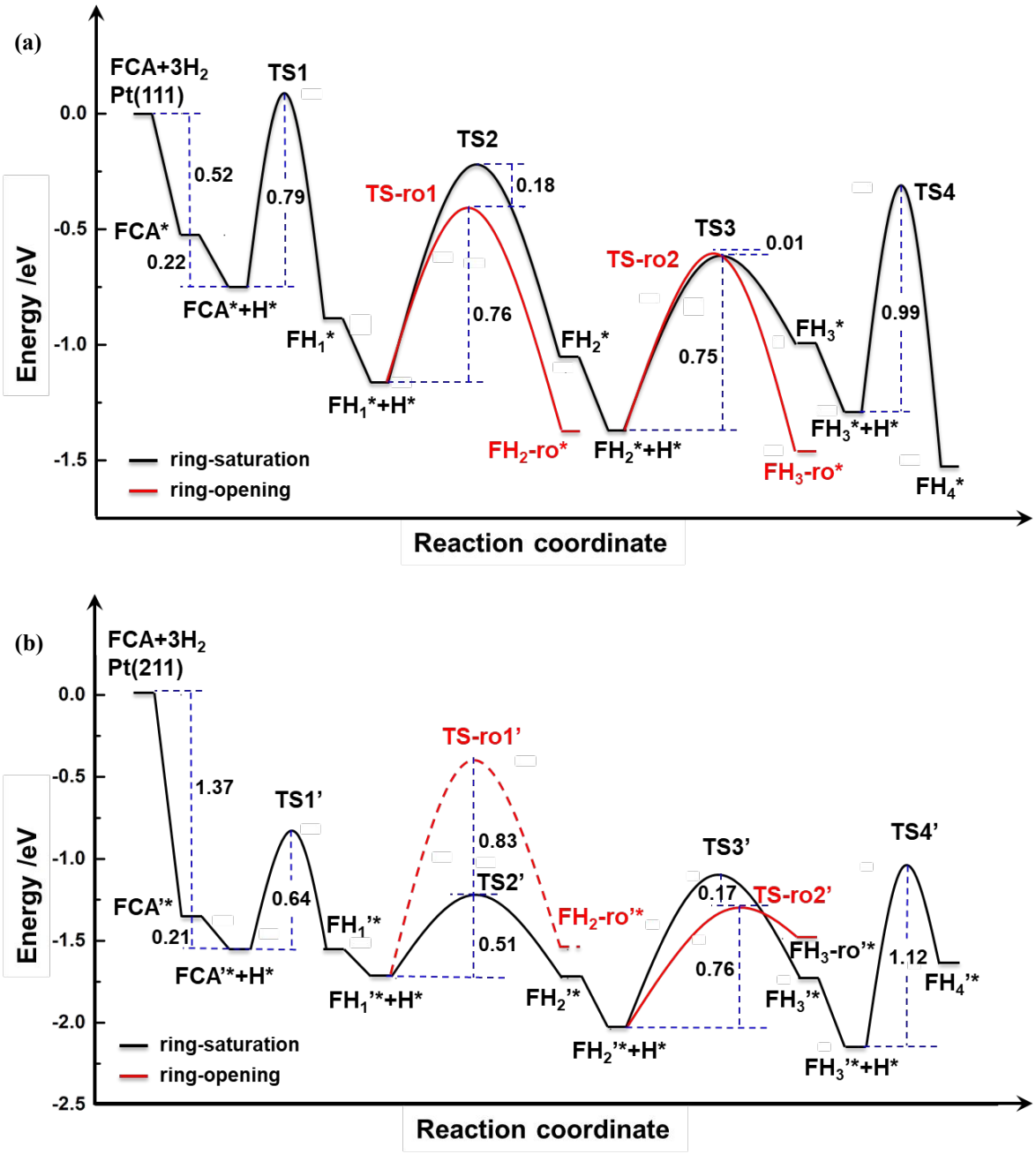

Figure 8. Calculated energy profiles for possible ring-saturation (black line) and ring-opening (red line) pathways in FCA hydrogenolysis on (a) Pt(111) surface and (b) Pt(211) surface.

FCA hydrogenolysis on the Pt(111) surface is initiated by the attack of a H atom to the adsorbed FCA species. This H atom can either be added to one of the four C atoms in the furan ring (C2-C5, labeled in Fig. 7) for ring saturation or the furan-ring O atom for C-O

bond cleavage. DFT-derived changes of reaction energies and activation barriers show that the first H-addition prefers the C4 position both kinetically and thermodynamically (see details in Table S1, SI). On the other hand, the transition state (denoted as TS1 in Fig. 8a) for the H-addition at the C4 position has significantly higher energy (0.05 eV, referred to a bare Pt surface and gaseous FCA and H_2 reactants) than those involved in the following FCA hydrogenation steps (TS2, TS3, and TS4 in Fig. 8a) as discussed below, indicative of kinetic relevance of this step on the Pt(111) surface.

Subsequent reaction of the surface species formed from the H-addition of FCA at the C4 position (denoted as FH_1*) with a second H atom has several possible products. DFT calculations show that the attacks of the second H atom at the other three C positions in the furan ring have similar activation barriers (E_a: 0.94-0.99 eV, with respect to FH_1* and H*; Table S2, SI), in which the C5 position (through TS2 in Fig, 8a; DFT-structure shown in Fig. 9a) is slightly preferred over the other two C positions, consistent with the relatively higher stability of the H-addition product at the C5 position (i.e. 4,5-dihydrofuran-2-carboxylic acid, denoted here as FH_2*). In contrast, the attacks at the O position of the furan ring lead to cleavages of the O1-C2 or O1-O5 bonds with activation barriers of 0.76 eV (TS-ro1 in Fig, 8a; DFT-structure shown in Fig. 9a) and 0.83 eV (details in Table S2, SI), respectively. The difference between these activation barriers for the O-C bond cleavage is attributed to the electron-withdrawing effect of the carboxylic group attached to the C2 position, reflecting that FCA is an inherently selective precursor for the formation of 5-HVA via hydrogenolysis. Moreover, these ring-opening activation barriers are lower than those for the ring saturation channels of FH_1*, which indicates that C-O bond cleavage is kinetically favorable compared

to the ring-saturation on the Pt(111) surface, consistent with the experimental observations (Section 3.1).

DFT-derived activation barriers for the H-addition of FH_2* show that the C2 position (through TS3 in Fig, 8a; DFT-structure shown in Fig. 9a) is preferred over the C3 position in accepting the third H atom for ring-saturation (E_a: 0.75 vs. 1.02 eV; Table S3, SI), while the competitive H addition to the O1 position of FH_2* mostly leads to cleavage of the O1-C2 bond with an activation barrier of 0.76 eV (TS-ro2 in Fig, 8a; DFT-structure shown in Fig. 9a). The similar activation barriers for the ring-saturation and ring-opening pathways of FH_2* imply that FH_2* would contribute equally to the selectivities of the THFCA and 5-HVA products. On the other hand, the product of H addition to the C2 position of FH_2* (denoted as FH_3*) can further react with the fourth H atom at the C3 position to form THFCA (E_a: 0.99 eV). However, this intermediate has to overcome a much higher barrier for the H attack at the O1 position, because of the large distance of the O1 atom in FH_3* from the Pt(111) surface (0.39 nm, Fig. S11, SI). Taken together, FH_2* and FH_3* are excluded as the key intermediates that determine the selectivities of THFCA and 5-HVA on Pt(111) surface, which in turn suggests the preference of O1-C2 bond cleavage in FH_1* hydrogenation accounts for the high selectivity of 5-HVA on the low-index Pt(111) surface.

DFT-derived ring-saturation and ring-opening pathways for FCA hydrogenation on Pt(211) surface (Fig. 8b) are similar to those found for Pt(111). Specifically, the first H atom prefers to attack the C3 and C4 positions with similar activation energies of 0.64 eV (Table S4, SI). As for the Pt(111) surface, the first H-addition step appears to be the kinetically relevant step for FCA hydrogenation on Pt(211), as evidenced from the relatively higher

energy of the transition state (TS1') of this step compared to those involved in the subsequent H-addition steps (TS2', TS3' and TS4' in Fig. 8b). However, the transition state (TS1' in Fig. 8b) of the H-addition on Pt(211) is more stable than that (TS1 in Fig.8a) on Pt(111) by 0.99 eV (referred to the corresponding bare Pt surface and gaseous FCA and H_2 reactants), reflecting the stronger bonding of such transition states to the step sites exposed on the Pt(211) surface. This stability difference of the kinetically-relevant H-addition transition states on Pt surfaces, mainly ascribed to the difference of the electronic density between the step and terrace sites, is consistent with the higher FCA hydrogenolysis activity measured on the higher-index Pt surfaces (Section 3.3).

DFT calculations suggest that the preferential sequence of the H addition positions for ring saturation of FCA on the stepped Pt(211) surface follows C4→C3→C5→C2 (detailed results shown in Table S4-S6, SI), whereas the corresponding sequence on the flat Pt(111) surface is C4→C5→C2→C3 as described above. Here, FH_n'* is denoted as the corresponding product formed after the addition of the *n*th H atom on the Pt(211) surface. Analogous to the branching ring-saturation and ring-opening pathways on Pt(111), FH_1'* and FH_2'* are the reaction intermediates relevant to the selectivities of THFCA and 5-HVA. As shown in Figure 8b, the activation barriers for ring-saturation and ring-opening of FH_1'* are 0.51 and 1.34 eV (TS2' vs. TS-ro1' in Fig. 8b; DFT-structure shown in Fig. 9b), respectively, implying the preference of FH_1'* to form THFCA. In contrast, the two activation barriers for FH_2'* is inverted (TS3': 0.93 eV vs. TS-ro2': 0.76 eV, Fig. 8b; DFT-structure shown in Fig. 9b), which results in its ring-opening and the favored formation of 5-HVA over THFCA on Pt(211).

As demonstrated above, the FH_1* and FH_2* intermediates contribute to the formation of 5-HVA from FCA hydrogenolysis on Pt(111), whereas FH_2'* is nearly the sole intermediate that leads to the formation of 5-HVA on Pt(211). Therefore, the Pt(111) surface is more selective to 5-HVA than the stepped Pt(211) surface, although the activation barrier difference between the ring-saturation and ring-opening pathways for FH_1* on Pt(111) and FH_2'* on Pt(211) is similar (0.18 vs. 0.17 eV, Fig. 8). These DFT assessments are in good agreement with the experimental results, and also suggest that the high activation barrier for the C-O bond cleavage in FH_1'* hydrogenation accounts for the lower selectivity of 5-HVA on Pt(211) compared to Pt(111). DFT treatments reveal that such hydrogenative ring-opening reactions involve late transition states, in which the bond between the attacking H atom and the O1 atom of the furan ring is nearly fully formed and the O1-C2 bond of the furan ring is partially cleaved (TS-ro1, TS-ro2, TS-ro1' and TS-ro2' in Fig. 9). Accordingly, the stabilization of the dangling C2 atom by the surface Pt atoms at the transition state is critical to the activation barrier. On Pt(211) surfaces, the dangling C2 atom has to share a step Pt site with the unsaturated C3 atom of FH_1'*, because the neighboring Pt atoms of this step site are too far to form effective bonding with the C2 atom (distance > 0.32 nm, TS-ro1' in Fig. 9b). In contrast, the dangling C2 atom and the unsaturated C3 atom of FH_1* at the ring-opening transition state (TS-ro1 in Fig. 9a) can be stabilized by separate terrace Pt atoms on Pt(111) surfaces, benefiting from the flat nature of the low-index surface. We surmise that such coordination difference between the transition state and the Pt surface results in the different C-O cleavage activation barriers on the Pt(111) and Pt(211) surfaces, which finally leads to the observed higher 5-HVA selectivity on Pt(111). The above theoretical calculations thus

indicate the catalytic activity and selectivity of FCA hydrogenolysis on Pt surfaces are determined by the electronic and geometric factors of the Pt surface sites, respectively, providing guidance to the rational design of novel catalysts for selective hydrogenolysis of FCA and its derivatives.

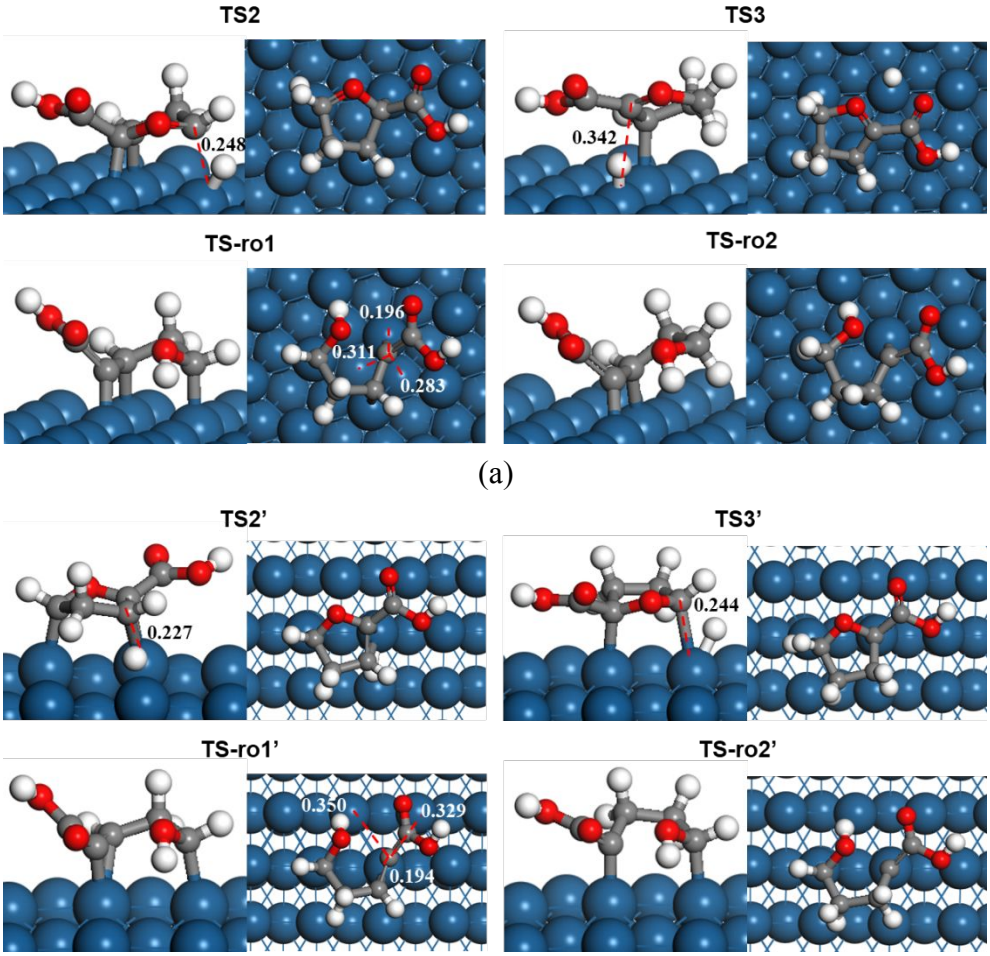

Figure 9. Calculated structures of transition states (a) TS2, TS3, TS_ro1, and TS_ro2 on Pt(111) surface and (b) TS2', TS3', TS-ro1', and TS-ro2' on Pt(211) surface (Atom legend: Pt, blue; C, gray; O, red; H, white).

4. CONCLUSIONS

The α-C-O bond of the furan ring is selectively cleaved in FCA hydrogenolysis to form 5-HVA in a high yield (~78%) on supported Pt catalysts at near-ambient temperature (i.e. 313

K). Spectroscopic assessment of exposed Pt sites shows that FCA hydrogenolysis turnover rate and 5-HVA selectivity are mediated by the ratio of low-index and high-index Pt surfaces on the catalysts; higher portion of low-index surfaces promotes the 5-HVA selectivity, but leads to low turnover rate. Kinetic assessment and theoretical calculations unveil that the addition of the first H atom to the unsaturated C atom of the adsorbed furan ring is the kinetically relevant step in FCA hydrogenolysis on Pt surfaces. The step sites predominantly present on high-index surfaces, compared to the terrace sites on low-index surfaces, tend to lower the energy of transition states in the kinetically relevant step, and thus facilitate the turnover rate; the terrace sites, together with the electron-withdrawing effect of the carboxylic substitute, favorably stabilize the dangling C2 atom of the transition states in ring-opening steps with lower activation barrier relative to the ring-saturation steps, and thus facilitates the α-C-O bond cleavage to form 5-HVA. This work provides an efficient way to produce high-valued C5 chemicals from bio-based feedstocks, and demonstrates the importance of controlling exposed metal catalyst surfaces and also intrinsic chemical properties of functional groups in the oxygenated reactants in the modulation of activity and selectivity.

ASSOCIATED CONTENT

AUTHOR INFORMATION

Corresponding Author

*E-mail: hcliu@pku.edu.cn.

Author Contributions

†Q.S. and S.W. contributed equally to this work.

Notes

The authors declare no competing financial interest.

Supporting Information

Dependence of product selectivities on FCA conversion; TEM micrographs and XRD patterns for spent Pt/SiO_2-4.2nm; effects of FCA and H_2 concentrations on the selectivity of FCA hydrogenolysis on Pt/SiO_2-4.2nm and Pt/TiO_2-2.0nm; Parity plots for the measured and predicted rates of FCA hydrogenolysis based on Eq.(4); calculated reaction energies (ΔE) and activation barriers (E_a) for elementary steps along the ring-saturation and ring-opening pathways on Pt(111) and Pt(211) surface; and calculated structures of absorbed FCA and possible intermediates on Pt(111) and Pt(211) surfaces.

ACKNOWLEDGMENT

This work was supported by the National Key Research and Development Program of China (2016YFB0701100), the Natural Science Foundation of China (21433001, 21690081, 21832001, 21821004, and 21805309), and Beijing National Laboratory for Molecular Sciences (BNLMS-CXXM-201905).

REFERENCES

1. Van de Vyver, S.; Román-Leshkov, Y. Emerging catalytic processes for the production of adipic acid. *Catal. Sci. Technol.* **2013,** *3*, 1465-1479.
2. Ji, X.; Huang, H. In *Bioprocessing of Renewable Resources to Commodity Bioproducts*, Bisaria, V. S., Kondo, A., Eds. John Wiley & Sons, Inc.: 2014; pp 261-288.
3. Corma, A.; Iborra, S.; Velty, A. Chemical routes for the transformation of biomass into chemicals. *Chem. Rev.* **2007,** *107*, 2411-2502.

4. Gallezot, P. Conversion of biomass to selected chemical products. *Chem. Soc. Rev.* **2012,** *41*, 1538-1558.
5. Besson, M.; Gallezot, P.; Pinel, C. Conversion of Biomass into Chemicals over Metal Catalysts. *Chem. Rev.* **2014,** *114*, 1827-1870.
6. Ide, M. S.; Davis, R. J. Perspectives on the kinetics of diol oxidation over supported platinum catalysts in aqueous solution. *J. Catal.* **2013,** *308*, 50-59.
7. Nakagawa, Y.; Tamura, M.; Tomishige, K. Catalytic Reduction of Biomass-Derived Furanic Compounds with Hydrogen. *ACS Catal.* **2013,** *3*, 2655-2668.
8. Li, X.; Jia, P.; Wang, T. Furfural: A Promising Platform Compound for Sustainable Production of C4 and C5 Chemicals. *ACS Catal.* **2016,** *6*, 7621-7640.
9. Xu, W.; Wang, H.; Liu, X.; Ren, J.; Wang, Y.; Lu, G. Direct catalytic conversion of furfural to 1,5-pentanediol by hydrogenolysis of the furan ring under mild conditions over Pt/Co_2AlO_4 catalyst. *Chem. Commun.* **2011,** *47*, 3924-3926.
10. Mizugaki, T.; Yamakawa, T.; Nagatsu, Y.; Maeno, Z.; Mitsudome, T.; Jitsukawa, K.; Kaneda, K. Direct Transformation of Furfural to 1,2-Pentanediol Using a Hydrotalcite-Supported Platinum Nanoparticle Catalyst. *ACS Sustainable Chem. Eng.* **2014,** *2*, 2243-2247
11. Tong, T.; Xia, Q.; Liu, X.; Wang, Y. Direct hydrogenolysis of biomass-derived furans over Pt/CeO_2 catalyst with high activity and stability. *Catal. Commun.* **2017,** *101*, 129-133.
12. Zhang, B.; Zhu, Y. L.; Ding, G. Q.; Zheng, H. Y.; Li, Y. W. Selective conversion of furfuryl alcohol to 1,2-pentanediol over a Ru/MnO_x catalyst in aqueous phase. *Green Chem.* **2012,** *14*, 3402-3409.
13. Liu, H.; Huang, Z.; Zhao, F.; Cui, F.; Li, X.; Xia, C.; Chen, J. Efficient hydrogenolysis of biomass-derived furfuryl alcohol to 1,2- and 1,5-pentanediols over a non-precious Cu–$Mg_3AlO_{4.5}$ bifunctional catalyst. *Catal. Sci. Technol.* **2016,** *6*, 668-671.
14. Ma, R.; Wu, X.-P.; Tong, T.; Shao, Z.-J.; Wang, Y.; Liu, X.; Xia, Q.; Gong, X.-Q. The Critical Role of Water in the Ring Opening of Furfural Alcohol to 1,2-Pentanediol. *ACS Catal.* **2017,** *7*, 333-337.
15. Sulmonetti, T. P.; Hu, B.; Lee, S.; Agrawal, P. K.; Jones, C. W. Reduced Cu–Co–Al Mixed Metal Oxides for the Ring-Opening of Furfuryl Alcohol to Produce Renewable Diols. *ACS Sustainable Chem. Eng.* **2017,** *5*, 8959-8969.
16. Wijaya, H. W.; Kojima, T.; Hara, T.; Ichikuni, N.; Shimazu, S. Synthesis of 1,5-Pentanediol by Hydrogenolysis of Furfuryl Alcohol over Ni–Y_2O_3 Composite Catalyst. *ChemCatChem* **2017,** *9*, 2869-2874.
17. Tong, T.; Liu, X.; Guo, Y.; Norouzi Banis, M.; Hu, Y.; Wang, Y. The critical role of CeO_2 crystal-plane in controlling Pt chemical states on the hydrogenolysis of furfuryl alcohol to 1,2-pentanediol. *J. Catal.* **2018**, *365*, 420-428.
18. Koso, S.; Ueda, N.; Shinmi, Y.; Okumura, K.; Kizuka, T.; Tomishige, K. Promoting effect of Mo on the hydrogenolysis of tetrahydrofurfuryl alcohol to 1,5-pentanediol over Rh/SiO_2. *J. Catal.* **2009,** *267*, 89-92.
19. Brentzel, Z. J.; Barnett, K. J.; Huang, K.; Maravelias, C. T.; Dumesic, J. A.; Huber, G. W. Chemicals from Biomass: Combining Ring-Opening Tautomerization and Hydrogenation Reactions to Produce 1,5-Pentanediol from Furfural. *ChemSusChem* **2017,** *10*, 1351-1355.
20. Chia, M.; Pagán-Torres, Y. J.; Hibbitts, D.; Tan, Q.; Pham, H. N.; Datye, A. K.;

Neurock, M.; Davis, R. J.; Dumesic, J. A. Selective Hydrogenolysis of Polyols and Cyclic Ethers over Bifunctional Surface Sites on Rhodium–Rhenium Catalysts. *J. Am. Chem. Soc.* **2011,** *133*, 12675-12689.

21. Chen, K.; Mori, K.; Watanabe, H.; Nakagawa, Y.; Tomishige, K. C–O bond hydrogenolysis of cyclic ethers with OH groups over rhenium-modified supported iridium catalysts. *J. Catal.* **2012,** *294*, 171-183.

22. Verdeguer, P.; Merat, N.; Gaset, A. Lead/platinum on charcoal as catalyst for oxidation of furfural. Effect of main parameters. *Appl. Catal., A* **1994,** *112*, 1-11.

23. Verdeguer, P.; Merat, N.; Rigal, L.; Gaset, A. Optimization of experimental conditions for the catalytic-oxidation of furfural to furoic acid. *J. Chem. Technol. Biotechnol.* **1994,** *61*, 97-102.

24. Tian, Q.; Shi, D.; Sha, Y. CuO and Ag_2O/CuO catalyzed oxidation of aldehydes to the corresponding carboxylic acids by molecular oxygen. *Molecules* **2008,** *13*, 948-957.

25. Firlotte, N.; Cooper, D. G.; Maric, M.; Nicell, J. A. Characterization of 1,5-Pentanediol Dibenzoate as a Potential "Green" Plasticizer for Poly(vinyl chloride). *J. Vinyl Addit. Technol.* **2009,** *15*, 99-107.

26. Wyatt, V. T. Effects of swelling on the viscoelastic properties of polyester films made from glycerol and glutaric acid. *J. Appl. Polym. Sci.* **2012,** *126*, 1784-1793.

27. Vidyasagar, A.; Ku, S. H.; Kim, M.; Kim, M.; Lee, H. S.; Pearce, T. R.; McCormick, A. V.; Bates, F. S.; Kokkoli, E. Design and Characterization of a PVLA-PEG-PVLA Thermosensitive and Biodegradable Hydrogel. *ACS Macro Lett.* **2017,** *6*, 1134-1139.

28. Asano, T.; Tamura, M.; Nakagawa, Y.; Tomishige, K. Selective Hydrodeoxygenation of 2-Furancarboxylic Acid to Valeric Acid over Molybdenum-Oxide-Modified Platinum Catalyst. *ACS Sustainable Chem. Eng.* **2016,** *4*, 6253-6257.

29. Asano, T.; Nakagawa, Y.; Tamura, M.; Tomishige, K. Structure and Mechanism of Titania-Supported Platinum–Molybdenum Catalyst for Hydrodeoxygenation of 2-Furancarboxylic Acid to Valeric Acid. *ACS Sustainable Chem. Eng.* **2019,** *7*, 9601-9612.

30. Rioux, R. M.; Song, H.; Hoefelmeyer, J. D.; Yang, P.; Somorjai, G. A. High-surface-area catalyst design: Synthesis, characterization, and reaction studies of platinum nanoparticles in mesoporous SBA-15 silica. *J. Phys. Chem. B* **2005,** *109*, 2192-2202.

31. Kresse, G.; Hafner, J. Ab initio molecular-dynamics simulation of the liquid-metal--amorphous-semiconductor transition in germanium. *Phys. Rev. B* **1994,** *49*, 14251-14269.

32. Kresse, G.; Furthmüller, J. Efficiency of ab-initio total energy calculations for metals and semiconductors using a plane-wave basis set. *Comput. Mater. Sci.* **1996,** *6*, 15-50.

33. Perdew, J. P.; Burke, K.; Ernzerhof, M. Generalized Gradient Approximation Made Simple. *Phys. Rev. Lett.* **1996,** *77*, 3865-3868.

34. Kresse, G.; Joubert, D. From ultrasoft pseudopotentials to the projector augmented-wave method. *Phys. Rev. B* **1999,** *59*, 1758-1775.

35. Monkhorst, H. J.; Pack, J. D. Special points for Brillouin-zone integrations. *Phys. Rev. B* **1976,** *13*, 5188-5192.

36. Henkelman, G.; Jónsson, H. Improved tangent estimate in the nudged elastic band method for finding minimum energy paths and saddle points. *J. Chem. Phys.* **2000,** *113*, 9978-9985.

37. Henkelman, G.; Jónsson, H. A dimer method for finding saddle points on high dimensional potential surfaces using only first derivatives. *J. Chem. Phys.* **1999,** *111*, 7010-7022.
38. Kittel, C. *Introduction to Solid State Physics*. John Wiley & Sons Ltd: New York, 1996.
39. Hibbitts, D.; Neurock, M. Promotional effects of chemisorbed oxygen and hydroxide in the activation of C–H and O–H bonds over transition metal surfaces. *Surf. Sci.* **2016**, *650*, 210-220.
40. Lamberti, C.; Zecchina, A.; Groppo, E.; Bordiga, S. Probing the surfaces of heterogeneous catalysts by in situ IR spectroscopy. *Chem. Soc. Rev.* **2010,** *39*, 4951-5001.
41. Raskó, J. CO-induced surface structural changes of Pt on oxide-supported Pt catalysts studied by DRIFTS. *J. Catal.* **2003,** *217*, 478-486.
42. Holmgren, A.; Andersson, B.; Duprez, D. Interactions of CO with Pt/ceria catalysts. *Appl. Catal., B* **1999,** *22*, 215-230.
43. Qiao, B.; Wang, A.; Yang, X.; Allard, L. F.; Jiang, Z.; Cui, Y.; Liu, J.; Li, J.; Zhang, T. Single-atom catalysis of CO oxidation using Pt1/FeOx. *Nat. Chem.* **2011,** *3*, 634.
44. Lu, C. M.; Lin, Y. M.; Wang, I. Naphthalene hydrogenation over Pt/TiO_2-ZrO_2 and the behavior of strong metal-support interaction (SMSI). *Appl. Catal., A* **2000,** *198*, 223-234.
45. Jeong, E. S.; Park, C. I.; Jin, Z. L.; Hwang, I. H.; Son, J. K.; Kim, M. Y.; Choi, J. S.; Han, S. W. Temperature-Dependent Local Structural Properties of Redox Pt Nanoparticles on TiO_2 and ZrO_2 Supports. *Catal. Lett.* **2015,** *145*, 971-983.
46. Kappers, M. J.; van der Maas, J. H. Correlation between CO frequency and Pt coordination number. A DRIFT study on supported Pt catalysts. *Catal. Lett.* **1991,** *10*, 365-373.
47. Zhu, Y.; Zaera, F. Selectivity in the catalytic hydrogenation of cinnamaldehyde promoted by Pt/SiO_2 as a function of metal nanoparticle size. *Catal. Sci. Technol.* **2014,** *4*, 955-962.
48. DeRita, L.; Dai, S.; Lopez-Zepeda, K.; Pham, N.; Graham, G. W.; Pan, X.; Christopher, P. Catalyst Architecture for Stable Single Atom Dispersion Enables Site-Specific Spectroscopic and Reactivity Measurements of CO Adsorbed to Pt Atoms, Oxidized Pt Clusters, and Metallic Pt Clusters on TiO_2. *J. Am. Chem. Soc.* **2017,** *139*, 14150-14165.
49. Lundwall, M. J.; McClure, S. M.; Goodman, D. W. Probing Terrace and Step Sites on Pt Nanoparticles Using CO and Ethylene. *J. Phys. Chem. C* **2010,** *114*, 7904-7912.
50. Lentz, C.; Jand, S. P.; Melke, J.; Roth, C.; Kaghazchi, P. DRIFTS study of CO adsorption on Pt nanoparticles supported by DFT calculations. *J. Mol. Catal. A: Chem.* **2017,** *426*, 1-9.
51. Wang, S.; Vorotnikov, V.; Vlachos, D. G. A DFT study of furan hydrogenation and ring opening on Pd(111). *Green Chem.* **2014,** *16*, 736-747.
52. Cai, Q.; Wang, J.; Wang, Y.; Mei, D. Mechanistic insights into the structure-dependent selectivity of catalytic furfural conversion on platinum catalysts. *AlChE J.* **2015,** *61*, 3812-3824.
53. Lv, C.; Yang, B.; Pang, X.; Wang, G. Reaction mechanism of ethylene glycol decomposition on Pt model catalysts: A density functional theory study. *Appl. Surf. Sci.* **2016,** *390*, 1015-1022.

TOC Graphic

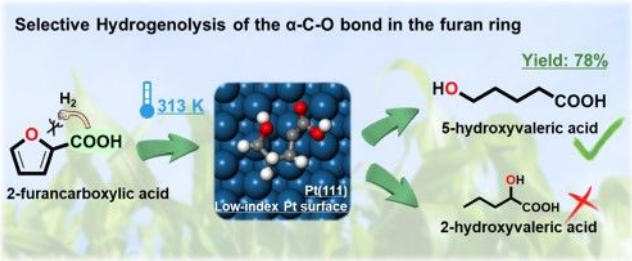
Selective Hydrogenolysis of the α-C-O bond in the furan ring
Yield: 78%
H2
COOH
2-furancarboxylic acid
313 K
Pt(111)
Low-index Pt surface
HO
COOH
5-hydroxyvaleric acid
OH
COOH
2-hydroxyvaleric acid